Figure S1. Related to Figure 1; Anesthetized recordings in MEC, further behavioral analysis, example histology, and cluster quality

(A) Example coronal slice showing viral expression and pipette track in dorso-medial entorhinal cortex for anesthetized recording experiments. GFP-conjugated Jaws was infused in three sites across the DV axis of MEC (see methods). Animals were left to recover for 4 weeks for optimal viral expression. For recording, the craniotomy was reopened and a optic-fiber-coupled recording pipette was lowered to MEC.
(B) Example recording sweep. Bottom: voltage trace for 35 second sweep, where the laser was triggered for ~5 seconds at ~5.5 seconds into the sweep. Top: tick-marks for action potentials from the cell recorded in the trace below.
(C) Mean temporal rate curves for all recorded cells (n=3), normalized by their peak firing rate across trials.
(D) Mean normalized firing rate during different segments of the recording for each pass (n=70). Firing rate is significantly lower within the laser window (signed-rank test).
(E) Analysis of error strategies during the behavioral task in Jaws Treadmill inactivation sessions. Plotted is the fraction of error trials that were followed by trials where the animal made the same choice. A fraction of zero would suggest the animals adopt an alternation strategy in response to errors, while a fraction of one would indicate perseveration. Animals' strategy did not change significantly between Baseline and intermixed Light-on/Light-off trials (17 sessions, signed rank test).
(F) Mean latency between the end of the treadmill delay and decision point (chosen as the time at which the animal begins to dig, or moves away from the pot toward the return arm of the maze). The mean decision latency increases in Light-on and Light-off, but these differences are not significant (17 sessions, signed rank test).
(G) As in **F**, but for the variance in decision latency for each trial type. Decision latency variance increases significantly for both Light-on and Light-off trials relative to Baseline levels (17 sessions, signed rank test). Inset: decision latency variance for each session, normalized by the trial type with greatest variance.
(**H)** As in **E** and **F**, but calculated separately for correct and incorrect trials. There is a selective increase in decision latency variance for incorrect trials during Light-on and Light-off trials (signed rank test).
(I) Histological summary for animals expressing the Jaws opsin in MEC. Scale bar is 2000μm.
(J) Analysis of cluster quality for identified time, place, and object selective cells used in the analysis. Units were well-isolated, and calculated L-ratios were uncorrelated to change in key analysis measures (Pearson's correlation).
Data are represented mean ± SEM, * $p < 0.05$, ** $p < 0.01$, *** $p < 0.001$.

Figure S2. Related to Figure 2 and 3; Effects of MEC inactivation on oscillatory dynamics and interneurons, and effect on temporal firing fields over successive trials

(A) Top: example raw (light grey) and theta-band filtered (dark grey, 4-12 Hz) local field potential recording during the treadmill delay for each trial type, from Jaws Treadmill inactivation sessions. Bottom: time-resolved Morlet wavelet spectrogram calculated across 150 linearly spaced frequencies from 1-90 Hz.

(B) Instantaneous theta band (4-12 Hz) power across the treadmill delay during Jaws Treadmill inactivation sessions. One wire with the highest average baseline theta power was chosen per session, and instantaneous theta power was derived via Hilbert transform and average across trials. Plotted are the mean ± SEM over time of the session trial type averages (17 sessions). There is no significant difference in time-resolved theta power between trial types (repeated measures ANOVA, $F_{trial\ type}$=0.19, p=0.66).

(C) As in C, but for high gamma band (60-90 Hz) power during the treadmill delay. There is no significant difference in time-resolved high gamma power between trial types (repeated measures ANOVA, $F_{trial\ type}$=0.09, p=0.76).

(D) Mean firing rate of putative interneurons for segments of their tuning curves between 0-2 sec, 2-4 sec, and 4-7 sec of the delay. In Jaws Treadmill inactivation sessions. There is no change in mean firing rate for activity in any timeblock of the delay (signed rank test).

(E) Percent change in interneuron firing rate variance across trials from Baseline as a function of time during the delay, for Light-on and Light-off trials (mean and 95% bootstrap confidence interval). Black asterisks indicate time periods where change in variance is significantly different than zero ($p<0.05$, bootstrap test). Interneurons exhibit elevated variance levels in response to and following MEC inactivation, though in a less time-locked fashion than pyramidal cells (main text Figure 3).

(F) Summary of interneuron firing rate variance changes from Baseline in different inactivation paradigms, for Light-on and Light-off trials. Only Jaws Treadmill phase inactivation sessions showed significant increases in interneuron firing rate variance compared to GFP controls (KW test, black asterisks indicate significant Tukey's *post hoc* test compared to GFP-only controls; gold asterisks indicate the median change in variance is significantly different from zero, p-value from 10,000 shuffles of trial-type identities; gold bar indicates 95th percentile of the null distribution).

(G) Temporal information for cells with significant temporal firing fields, calculated in a rolling 25% of trials advanced in 5% steps across trial types, shown separately for cells with Baseline peak average firing rate in 0-2 sec, 4-2 sec, or 4-7 sec portion of the treadmill delay during Jaws Treadmill inactivation sessions. Inset: Pearson correlation of the mean information curve with trial percentile. Mean information content does not recover and continues to decrease over the course of intermixed Light-on and Light-off trials for 0-2 and 4-7 sec peak cells. Information for 2-4 sec cells, whose firing fields reside within the temporal coverage of the laser, decreases abruptly during early Light-off trials and does not trend downward, while information during Light-on trials decreases abruptly and trends further downward on successive Light-on trials.

(H) Per-cell trends in information over successive trials, calculated as the Pearson correlation of each cell's information curve with trial percentile. Information trend is varied at the single-cell level, though 0-2 and 4-7 sec cells show significant downward information trends during Light-on trials, and 0-2 sec cells show significant downward information trends during Light-off trials (bootstrap test).

Data are represented mean ± SEM (B-D, G), or mean and 95% bootstrapped confidence interval (E, H); box and whiskers are IQR and 1.5 x IQR respectively; * $p< 0.05$, ** $p < 0.01$, *** $p <0.001$.

Figure S3. Related to Figures 2 and 3; MEC inactivation during Maze/Object phases does not affect Treadmill temporal coding

(A) Maze schematic illustrating the recording and optogenetic setup for Jaws Maze inactivation session: depicted analysis is for temporal firing fields on the treadmill (purple) during sessions where the laser was triggered on the return arm of the maze (red). 14 sessions.

(B) Reconstruction error for temporal decoding during the treadmill shown for Baseline (blue), Light-on (red), and Light-off (green) spikes, using the Baseline tuning curves as a template (as in Figures 2, see methods). The mean error in all trial types is significantly lower than the null distribution of mean errors from decoding with shuffled templates (p-value from 10,000 shuffles, compare to Figure 2D; see also Figure 2E).

(C) Temporal information (signed rank test), field stability (signed rank test), and mean firing rate (KS test) for all trial types, shown separately for cells with temporal firing fields that peak between 0-2, 2-4, and 4-7 sec of the treadmill delay. All unit metrics remain stable (compare to Figure 3B).

(D), (E), (F) As in **A**, **B**, **C**, for Jaws Object inactivation sessions, where we analyzed firing fields on the treadmill (purple) during sessions where the laser was triggered during the object sampling period (red). 15 sessions. Note though the decoding error in all trial types is significantly lower than the null distributions, the Light-on and Light-off error is higher than observed in other control types, similar to the slight expansion of the population temporal decorrelation interval for Jaws | Object sessions noted in main text Figure 4C. The small effect on time cell stability during object inactivation sessions may reflect the temporal proximity of these two task epochs during each trial.

(G), (H), (I) As in **A**, **B**, **C**, for GFP-control treadmill inactivation sessions, where we analyzed firing fields on the treadmill (purple) during sessions where the laser was triggered during the treadmill period (red) in animals whose viral construct lacked the Jaws opsin. 9 sessions.

Data are represented mean ± SEM, * $p < 0.05$, ** $p < 0.01$, *** $p < 0.001$.

Figure S4. Related to Figures 2 and 3; Treadmill-phase inactivation sessions exhibit similar levels of temporal coding across days; tetrode-collapsed data exhibits temporal coding deficits

(A) Fraction of recorded population exhibiting significant temporal tuning during Baseline across animals, for the first and second recording sessions (rank-sum test).

(B) Cumulative distribution of temporal information scores for significant cells recorded during Baseline for first and second recording sessions (rank-sum test).

(C) Animals' mean temporal information score for significant cells recorded during Baseline for first and second recording sessions (rank-sum test).

(D) Temporal information (top) and field stability (bottom) for cells in each time block of the delay during Jaws Treadmill inactivation session, recomputed using data from each unique tetrode only once (signed rank test). For each tetrode, we retained the cells that were recorded during the session where that tetrode recorded the most units.

(E) Percent change in firing rate variance across trials from Baseline as a function of time during the delay, for Light-on and Light-off trials. Mean firing rate variance curve was computed using one cell randomly drawn from each tetrode; this was repeated 1000 times to produce a mean subsampled curve and 95% confidence interval. Black asterisks indicate time periods where change in variance is significantly different than zero ($p<0.05$, bootstrap test).

(F) Summary of firing rate variance changes from Baseline in different inactivation paradigms, for Light-on and Light-off trials using tetrode-subsampled data in **E** (KW test, black asterisks indicate significant Tukey's *post hoc* test compared to GFP-only controls; gold asterisks indicate the median change in variance is significantly different from zero, p-value from 10,000 shuffles of trial-type identities; gold bar indicates 95th percentile of the null distribution).

Figure S5. Related to Figure 3; CA1 temporal coding disruption is not solely driven by reduced spiking

(A) Example single units during Jaws | Treadmill inactivation sessions. Note that two effect phenotypes can impair temporal coding: increased spiking variance without a reduction in mean firing rate (left-most two examples) or large reductions in mean firing rate (right-most two examples. Bottom row: spiking was randomly subsampled to equalize neurons' mean firing rate across Baseline, Light-on, and Light-off trial types (see methods).
(B) Example unit statistics (from the first and last units in **A**) calculated from 1000 sub-sampled simulations of the spiking data. Dashed line indicates the statistic calculated from the observed data. Solid line indicates the mean of the simulated distribution.
(C) Single unit analysis from main text Figure 3 recomputed with the mean simulated statistics for each cell (signed rank test). The firing-rate-equalized datasets exhibit comparable deficits in temporal coding to the observed data.
(D) Population vector analysis from main text Figure 4 recomputed with the mean simulated firing rate curves for each cell (signed rank test).
(E) Comparison between the observed change in mean firing rate between Light-on and Baseline, and the change in unit statistics between Light-on and Baseline, shown for the observed (green) and simulated (orange) spiking data. The line indicates the linear fit with the 68% confidence interval shaded. There is a weak relationship between firing rate and information change for the observed data that is reversed by the subsampling procedure (Pearson's correlation), though the marginal distributions of observed and simulated information scores are not significantly different (signed rank test). Changes in field stability do not exhibit a significant relationship to change in firing rate for either dataset.
(F) In order to directly compare whether changes in firing rate better predict changes in unit statistics for the observed or simulated data, we computed the magnitude of the difference between the coefficient of variation for each data set in E, and compared this value to a shuffled null distribution (see methods). There was no significant difference in prediction quality between the original and subsampled spiking, for either information or field stability. Data are represented mean ± SEM, * $p < 0.05$, ** $p < 0.01$, *** $p < 0.001$.

Figure S6. Related to Figures 5 and 6; MEC inactivation during Treadmill/Object phases does not affect Maze spatial coding

(A) Maze schematic illustrating the recording and optogenetic setup for Jaws Treadmill inactivation session: depicted analysis is for spatial firing fields on the return arm of the maze (purple) during sessions where the laser was triggered during the treadmill delay (red). 17 sessions.

(B) Reconstruction error for spatial decoding on the maze return arm shown for Baseline (blue), Light-on (red), and Light-off (green) spikes, using the Baseline tuning curves as a template (as in Figures 5, see methods). The mean error in all trial types is significantly lower than the null distribution of mean errors from decoding with shuffled templates (p-value from 10,000 shuffles, compare to Figure 5C; see also Figure 5D). 14 sessions.

(C) Spatial information (signed rank test), field stability (signed rank test), and mean firing rate (KS test) for all trial types. All unit metrics remain stable (compare to Figure 6B).

(D), (E), (F) As in **A**, **B**, **C**, for Jaws Object inactivation sessions, where we analyzed spatial firing fields on the maze return arm (purple) during sessions where the laser was triggered during the object sampling period (red).

(G), (H), (I) As in **A**, **B**, **C**, for GFP-control spatial inactivation sessions, where we analyzed spatial firing fields on the treadmill (purple) during sessions where the laser was triggered during one the maze return arm (red) in animals whose viral construct lacked the Jaws opsin. 8 sessions.

Data are represented mean ± SEM, * $p < 0.05$, ** $p < 0.01$, *** $p < 0.001$.

Figure S7. Related to Figures 7 and 8; MEC inactivation during Treadmill/Maze phases does affect Object-phase object coding; MEC inactivation does not differentially impact theta phase precession for object-selective spiking

(A) Maze schematic illustrating the recording and optogenetic setup for Jaws Treadmill inactivation session: depicted analysis is for object-selective firing during the object sampling period (purple) during sessions where the laser was triggered during the treadmill delay (red). 17 sessions.

(B) Cumulative distribution function for selectivity index (SI) p-values (left, see methods), and the fraction of cells with significant object selectivity in each trial type (right, Pearson's χ^2 test of independence, as in Figure 7C).

(C) SI values for cells with significant Baseline selectivity, compared across trial types (signed rank test, as in Figure 7D; see also Figure 7E).

(D), **(E)**, **(F)** As in **A**, **B**, **C**, for Jaws Maze inactivation sessions, where we analyzed object selective firing during the object sampling period (purple) during sessions where the laser was triggered on the return arm of the maze (red). 14 sessions.

(G), **(H)**, **(I)** As in **A**, **B**, **C**, for GFP Object inactivation sessions, where we analyzed object selective firing during the object sampling period (purple) during sessions where the laser was triggered during the object sampling period (red) in animals whose viral construct lacked the Jaws opsin. 6 sessions.

(J) Example highly-object selective cell, shown separately for object A (purple) and object B (orange) trials, and further split by Baseline (Blue), Light-on (Red), and Light-off (Green) trials. Each spike is plotted as a function of theta phase and time, and the smoothed firing rate curve and regression line (if significant circular-linear correlation, see methods) are overlaid. The cell shows a high preference for Object B, and exhibits theta phase precession during all trial types.

(K) Percent of significantly phase precessing cells (circular-linear correlation $p<0.05$, and a negative regression slope) during each trial type (Pearson's χ^2 test of independence).

(L) Slope of the circular-linear regression line for cells with significant precession in at least one trial type (signed rank test).

(M) Change in precession slope from Baseline for experimental and control groups (KW test).

* $p< 0.05$, ** $p < 0.01$, *** $p <0.001$.

SUPPLEMENTARY FIGURE 1

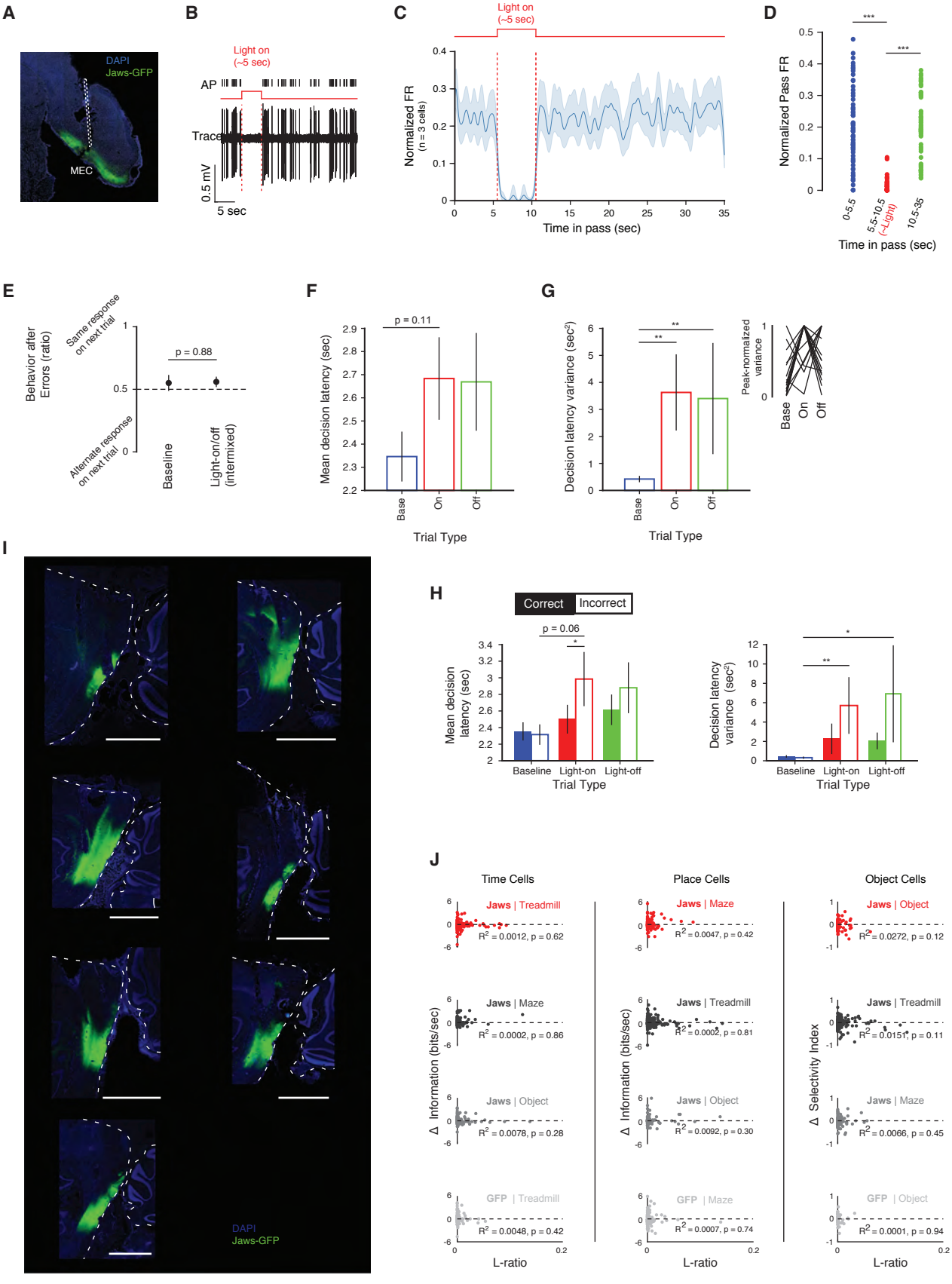

SUPPLEMENTARY FIGURE 2

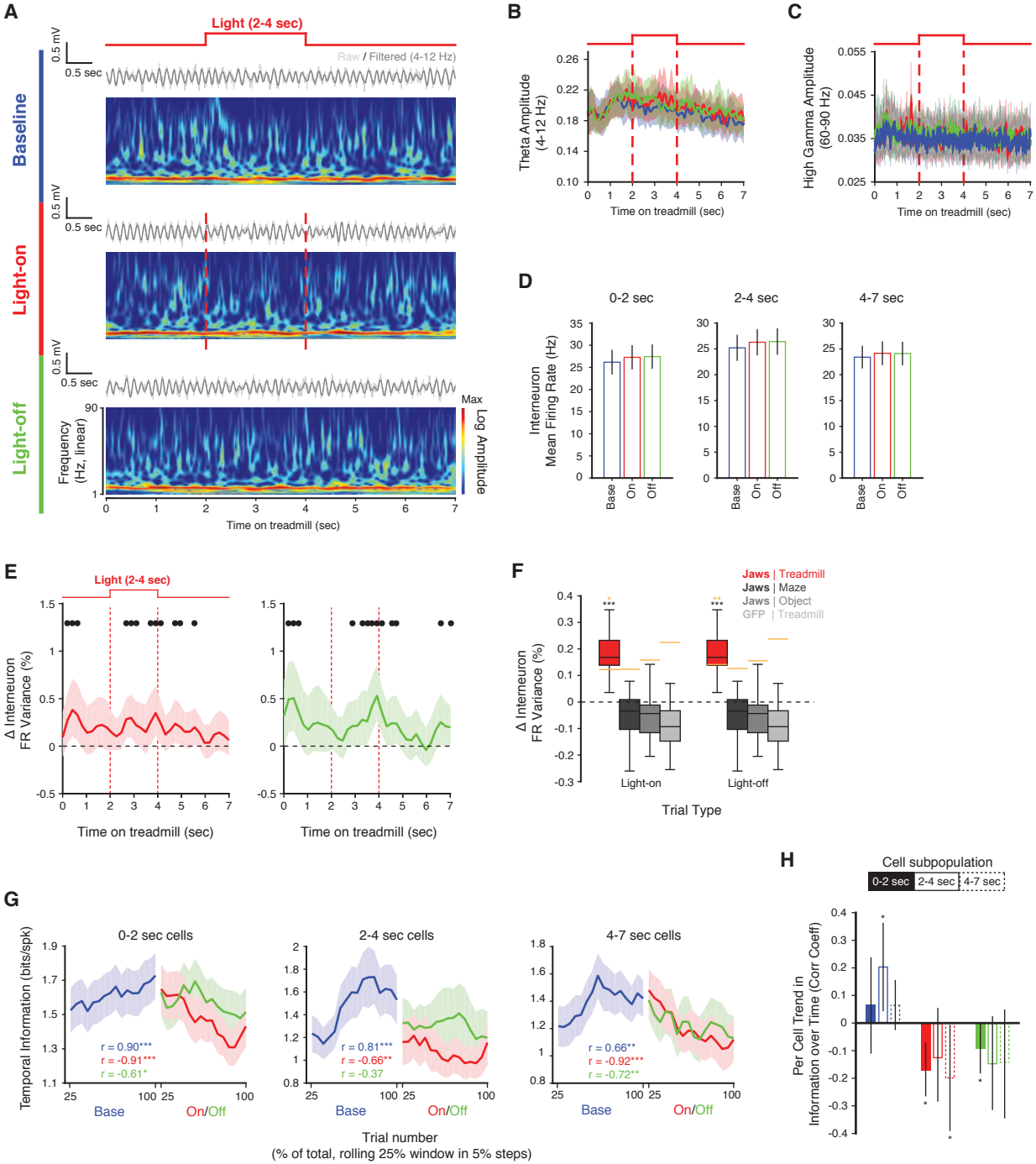

SUPPLEMENTARY FIGURE 3

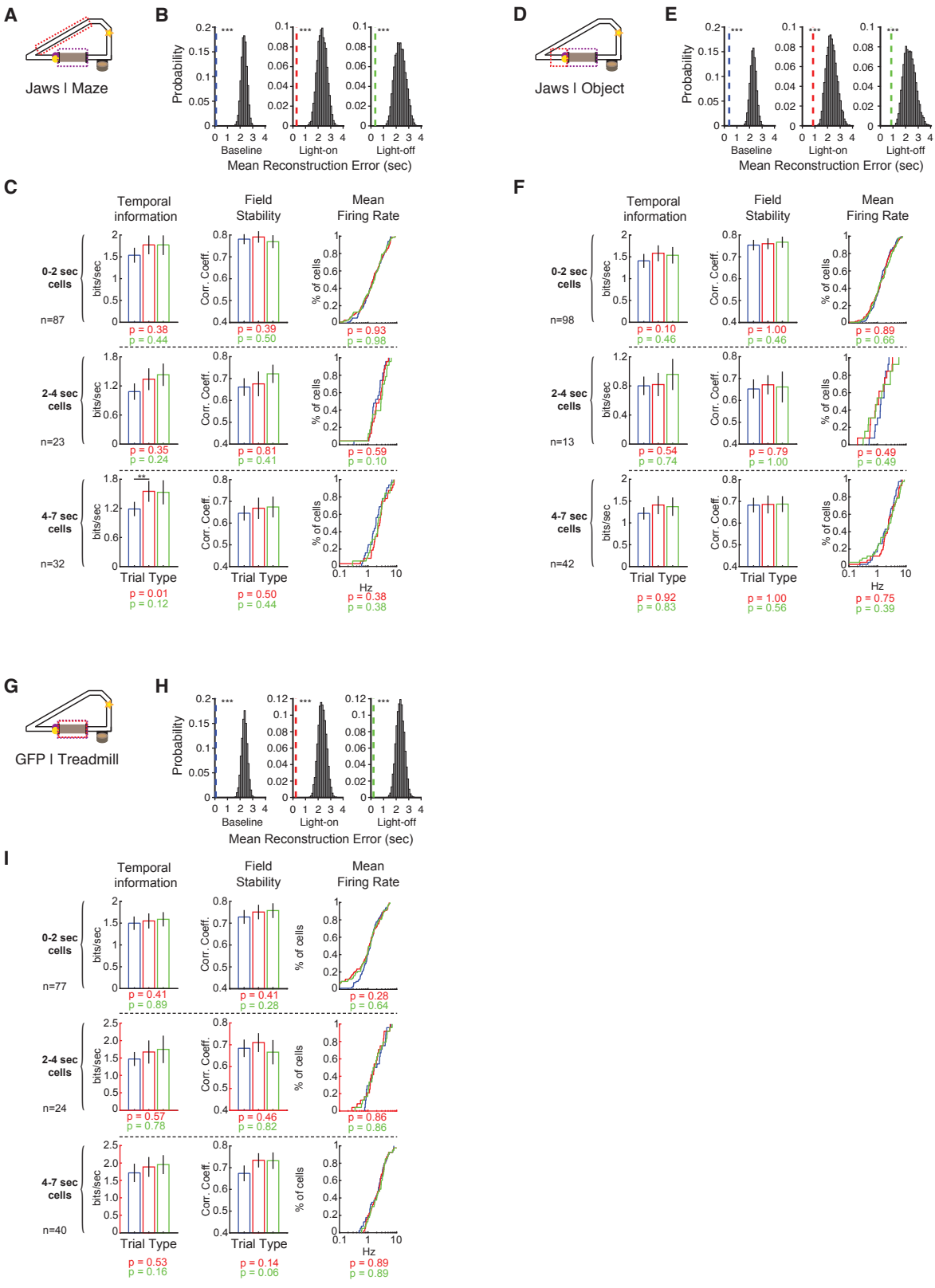

SUPPLEMENTARY FIGURE 4

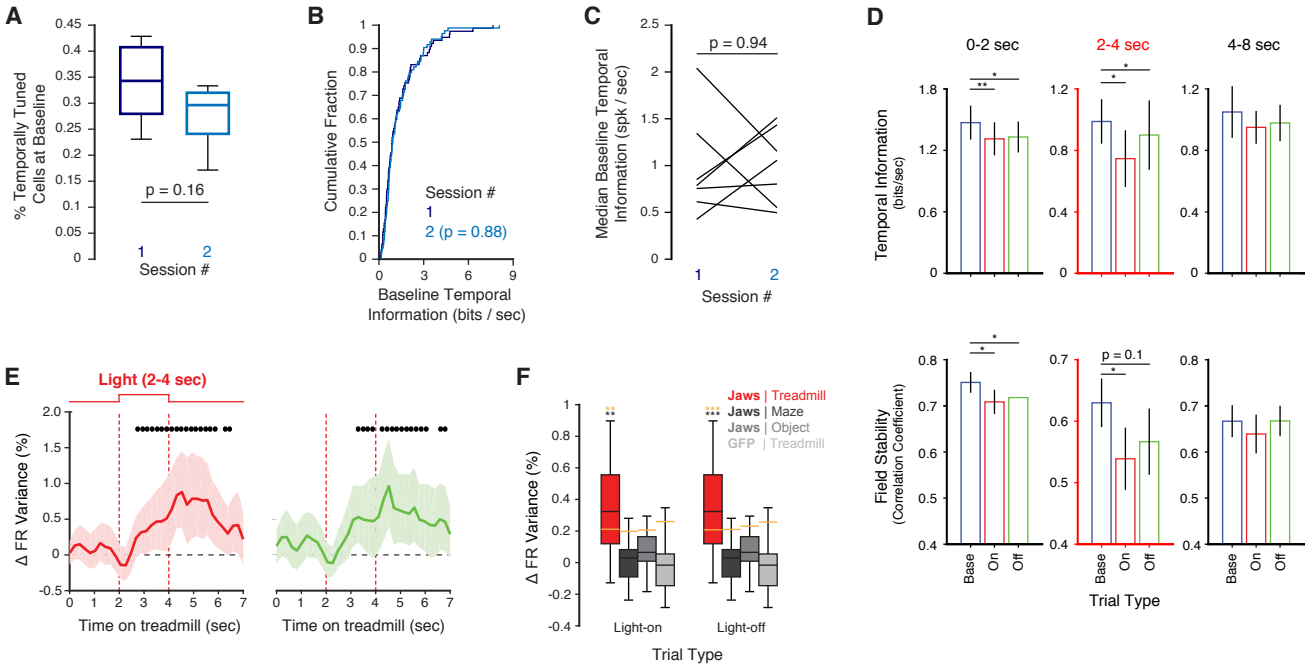

SUPPLEMENTARY FIGURE 5

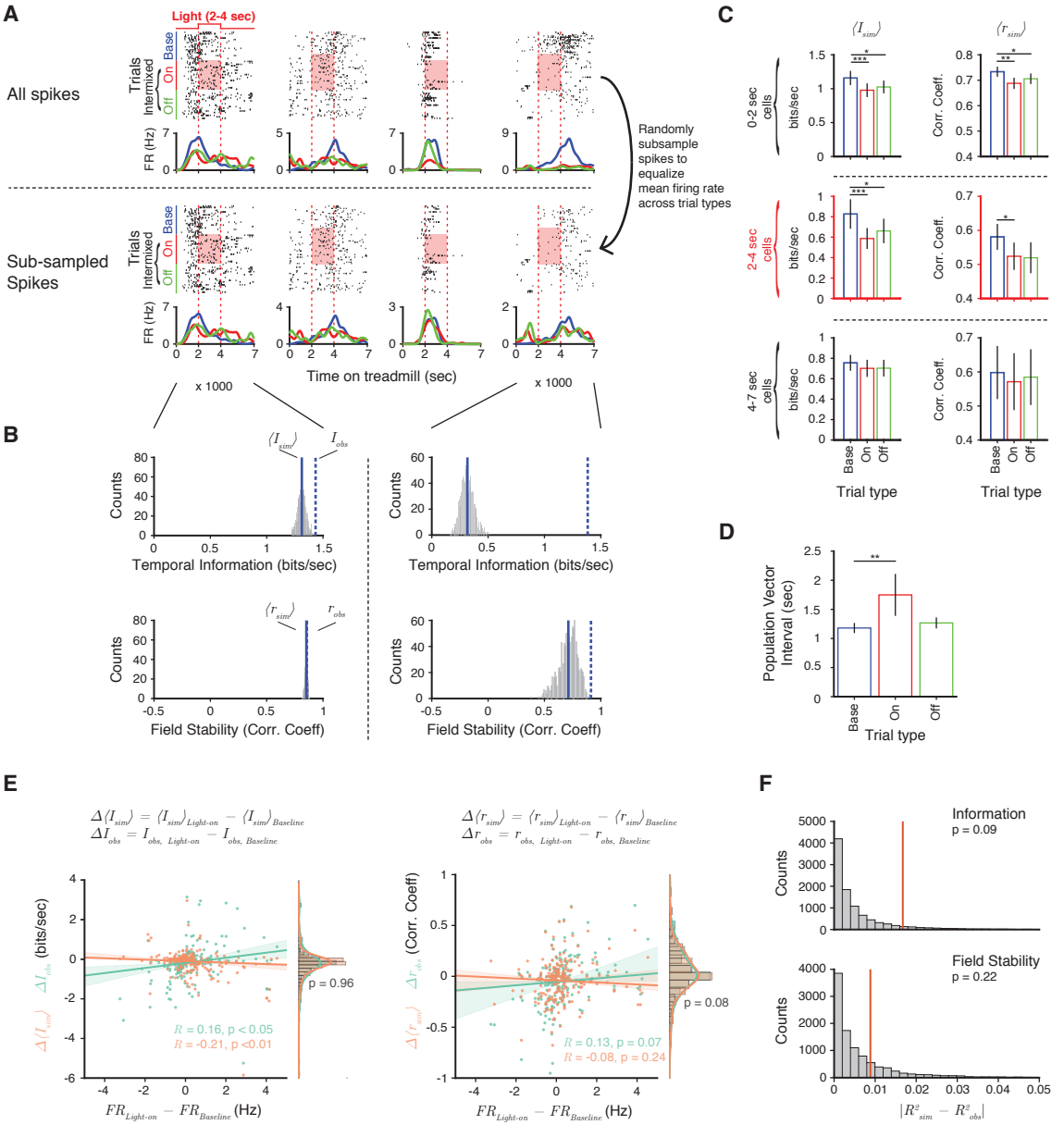

SUPPLEMENTARY FIGURE 6

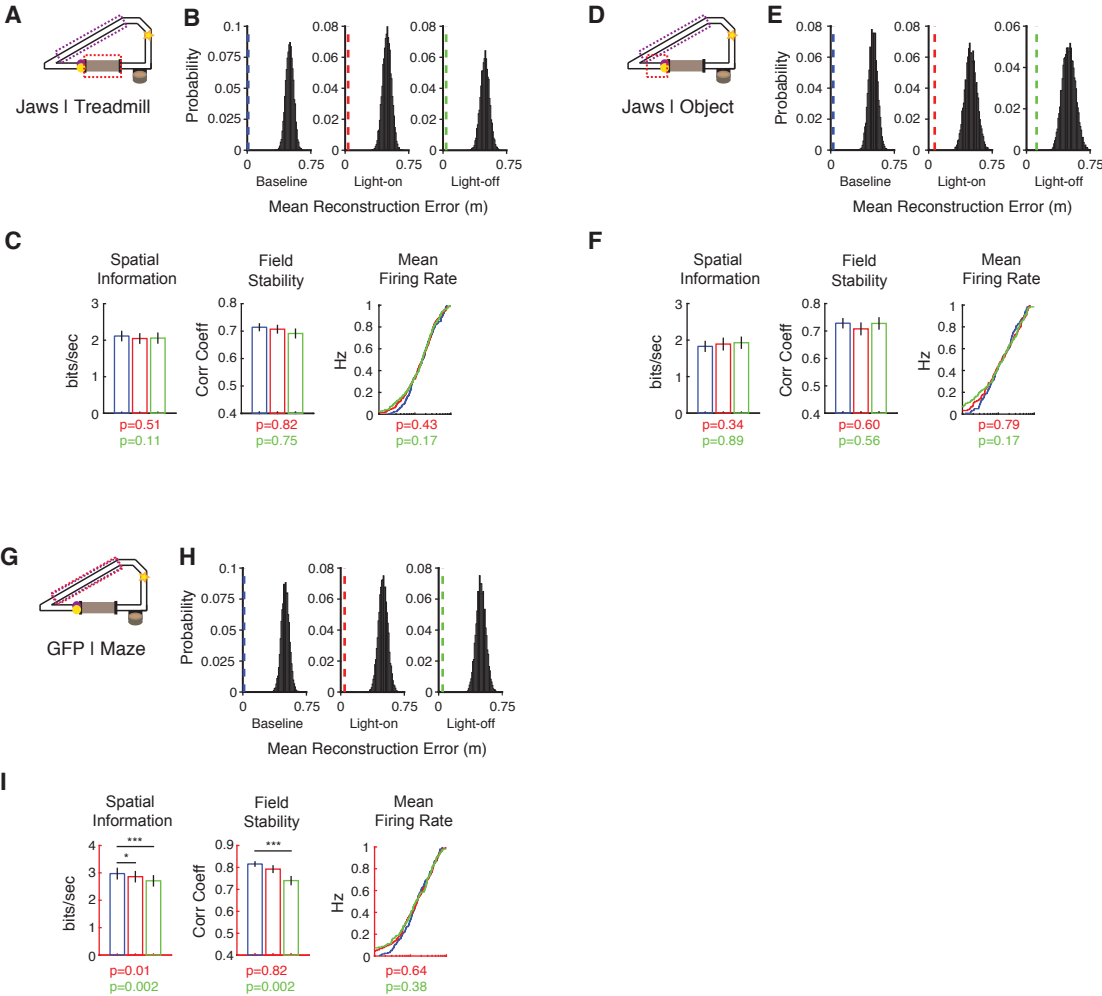

SUPPLEMENTARY FIGURE 7